SuperSpec: Development Towards a Full-Scale Filter Bank

J. Wheeler[a], S. Hailey-Dunsheath[b], E. Shirokoff[c], P. S. Barry[d], C. M. Bradford[e,b], S. Chapman[f], G. Che[g], J. Glenn[a], M. Hollister[b], A. Kovács[b,h], H. G. LeDuc[e], P. Mauskopf[g], R. McGeehan[c], C. M. McKenney[i], R. O'Brient [e], S. Padin[b], T. Reck[e], C. Ross[f], C. Shiu[b], C. E. Tucker[d], R. Williamson[e], and J. Zmuidzinas[b]

[a]Center for Astrophysics and Space Astronomy, University of Colorado Boulder, 2000 Colorado Avenue, Boulder 80309, USA
[b]California Institute of Technology, 1200 E. California Blvd, Mail Code 301-17, Pasadena 91125, USA
[c]Department of Astronomy & Astrophysics, University of Chicago, 5640 South Ellis Avenue, Chicago, IL 60637, USA
[d]School of Physics & Astronomy, Cardiff University, 5 The Parade, Cardiff CF24 3AA, UK
[f]Department of Physics and Atmospheric Science, Dalhousie University, Coburg Road, Halifax NS B3H 1A6, Canada
[g]School of Earth and Space Exploration and Department of Physics, Arizona State University, Tempe, AZ 85287, USA
[h]Institute for Astrophysics, University of Minnesota, 116 Church St SE, Minneapolis, MN 55455, USA
[e]Jet Propulsion Laboratory, 4800 Oak Grove Drive, Pasadena, CA 91109, USA
[i]National Institute of Standards and Technology, 325 Broadway, Boulder, CO 80305, USA

ABSTRACT

SuperSpec is a new spectrometer-on-a-chip technology for submm/mm-wave spectroscopy. SuperSpec stands out from other direct-detection submm spectrometer technologies in that the detectors are coupled to a series of resonant filters along a single microwave feedline instead of using dispersive optics. SuperSpec makes use of kinetic inductance detectors (KIDs) to detect radiation in this filter bank. The small profile of this design makes SuperSpec a natural choice to produce a multi-object spectrometer for tomographic mapping or galaxy redshift surveys. We have recently fabricated a device that is a 50 channel subset of a full 280 channel filter bank, which would cover the 190 - 310 GHz range at R = 275. Analysis of the data from this device informs us of the potential design modifications to enable a high-yield background-limited SuperSpec spectrometer. The results indicate that this subset filter bank can scale up to a full filter bank with only a few collisions in readout space and less than 20% variation in responsivity for the detectors. Additionally, the characterization of this and other prototype devices suggests that the noise performance is limited by generation-recombination noise. Finally, we find that the detectors are sufficiently sensitive for ground-based spectroscopy at R = 100, appropriate for tomographic mapping experiments. Further modifications are required to reach the background limit for R = 400, ideal for spectroscopy of individual galaxies.

Keywords: Kinetic Inductance Detectors, Millimeter-wave, TiN, Noise Equivalent Power, SuperSpec, Spectrometer, Filter-Bank, Critical Temperature

Further author information: (Send correspondence to J.D.W.)
J.D.W.: E-mail: Wheeler1711@gmail.com, Telephone: 1 314 574 1711

Millimeter, Submillimeter, and Far-Infrared Detectors and Instrumentation for Astronomy VIII,
edited by Wayne S. Holland, Jonas Zmuidzinas, Proc. of SPIE Vol. 9914, 99143K
 · doi: 10.1117/12.2233798

1. INTRODUCTION

The submm waveband contains a substantial fraction of the cosmic infrared background (CIB), which is the integrated light from luminous infrared galaxies at high redshift. It originates from the copious amount of energy produced by star formation and black hole accretion in the early Universe emitted as optical and ultraviolet (UV) light that was largely absorbed and re-emitted by interstellar dust in the far-infrared. The *Herschel Space Observatory* has revealed thousands of bright galaxies per deg^2 in the far-infrared.[1] To understand the star formation history of the Universe accurate redshifts are needed for these galaxies. The most unambiguous way to determine redshifts for these obscured, dusty galaxies is by measuring the rotational lines of CO and the far-infrared atomic fine structure lines. These lines also provide physical information about the galaxies, e.g. gas heating dynamics[2] and UV field hardness, which yields information about the nature of the embedded energy sources. ALMA has proved to be invaluable for measuring these attributes but lacks the spectral bandwidth to survey a large number of sources, and for all but the deepest integrations can only observe one galaxy at a time. This motivates the production of a survey instrument with a large instantaneous bandwidth and multi-object capability.

A wide-band integral field spectrometer also enables the study of the epoch of reionization via tomographic mapping of spectral lines. Between z = 6 and 20, the first stars began to form and enrich the Universe with heavy elements. This enabled further star formation, and along with black hole accretion, led to substantial UV flux that reionized the neutral Universe. Much of this UV flux is believed to originate from sub-dwarf galaxies with relatively low luminosities.[3] This makes observations of individual galaxies extremely difficult; however, it is possible to observe the cumulative flux for a spectral line at a given redshift, such as the 157.7 μm line of singly ionized carbon ([CII]). The power spectrum of a redshift/angular data cube measures the statistical properties of this population, such as the clustering of these galaxies, as well as the mean line intensity.[4]

The SuperSpec design is a filter bank much like those used in radio astronomy. The submm signal propagates down a feedline that is coupled to resonant filters that consist of $\lambda/2$ transmission lines, where λ is the central wavelength of radiation admitted by the filter. Each of the resonating filters is then coupled to a KID, which is in turn coupled to a microwave readout line.[5] The natural multiplexibilty of KIDs facilitates reading out spectrometers that each require 100s of detectors. The current device is a smaller subset (50 channels) of what would make up a full filter bank (∼280 channels) to target the 190-310 GHz atmospheric window at R = 275. The filter bank architecture and detector design are based on the 3^{rd} generation SuperSpec devices whose design is detailed in a previous paper.[6]

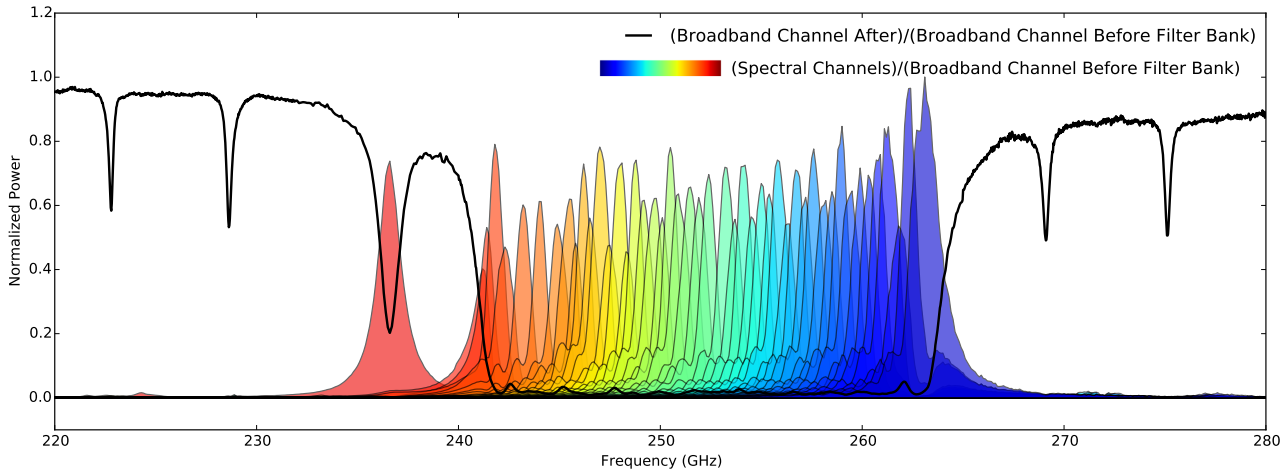

Figure 1. Optical profiles of the most recent SuperSpec device, a 50 channel filter bank with 100% yield. The black line shows a broadband channel at the end of the filter bank divided by a broadband channel at the front, approximating an S_{21} measurement. The colored profiles show the response of each resonator filter normalized by the broadband channel at the front of the filter bank, which removes the system's transfer function.

This paper discusses measurements of this 50 channel filter bank. The spectral profiles along with the total power absorbed is shown in Figure 1. The spectral filter channels span only a subset ($\sim$ 240-265 GHz) of the full (190-310 GHz) atmospheric window. These and other data are used to predict the performance of a full filter bank. For a full filter bank a high effective yield and sufficiently sensitive detectors are desired. The variation in critical temperature, T_c, across the device was examined to determine the impact on readout frequency scatter and responsivity variation. Next, the readout frequency scatter was examined in its entirety to predict the number of collisions for a full-scale filter bank. Additionally, the mm-wave filter frequency scatter was measured to determine the extent of overlapping channels or gaps in the spectral coverage. Finally, the limiting noise properties of the detectors were investigated as well as the achievable NEPs. The discussion of the spectral resolution, device loss, and total filter bank efficiency are left for a future paper.

2. T_C VARIATION ACROSS THE FILTER BANK

Variation across a wafer of the critical temperature, T_c, is an important issue for TiN KIDs. Non-uniform nitrogen concentrations in the deposition chamber during Ti sputtering cause a variation in the TiN stoichiometry, thereby causing a variation in T_c. A variation in T_c causes a change in the resonator readout frequency, which scales as $\sqrt{T_c}$. This can cause both wafer-level gradients and localized scatter in resonator readout frequencies, which may result in readout collisions for a KID array. Furthermore, variations in T_c cause variations in responsivity, which scale as $T_c^{3.5}$, meaning a 10% variation in T_c can cause a 40% variation in responsivity. One way this problem can be mitigated is by reducing the T_c variation across the chip. Methods to accomplish this include using a ring shaped nitrogen emitter, rather than a single source, while sputtering Ti (a method employed for this device), or by using multilayer films of alternating TiN and Ti.[7] Another way to reduce the effects of T_c variation is to place resonators that are near each other in readout space also near each other in physical space on the chip. This means that only the variation on very small scales is important for resonator frequency scatter and the large scale variation has minimal impact. This method has also been utilized for SuperSpec.

We estimate T_c by measuring the fractional frequency shift of resonators as a function of array temperature. Figure 2 shows the T_c variation for two recent SuperSpec filter bank devices. The first, Figure 2 (A), is the T_c variation for a filter bank for which the antenna did not yield in fabrication, making the device effectively dark. The mean T_c is consistent with the targeted value of 1.2 K adopted for our prototypes. The second, Figure 2 (B), is the T_c for the most recent optically active device where the T_c value was abnormally high.

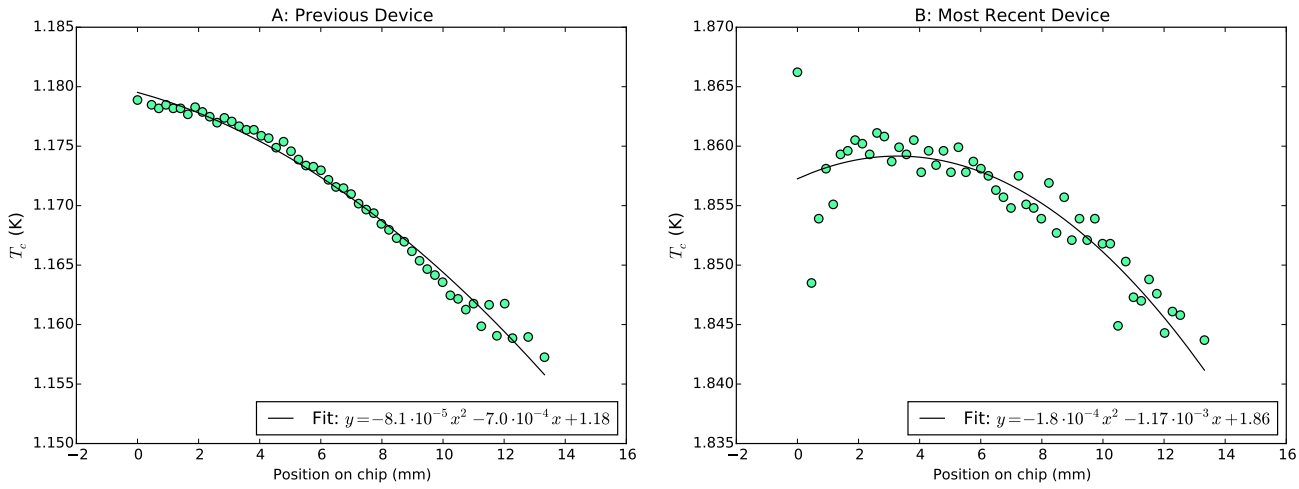

Figure 2. T_c as a function of chip position for two devices. (A) A previous device that was optically dark due to a lithography error. (B) Most recent optically active device that had an abnormally high T_c.

We found a 2% variation in T_c over a distance of 13 mm for the 50 channel filter bank. If this trend is extrapolated for a full 280 channel filter bank with the same $3\lambda/4$ spacing between resonant filters, the device

length would be 5.5 times greater. Then one might expect a 65% change in T_c across the device. However, extrapolating these data that far is most likely unreliable and we expect the variation will be smaller. In any case, such a large potential variation motivates decreasing the length of the filter bank on the wafer. This can be accomplished in two ways. One option for decreasing this variation would be to wrap the feedline in a two-dimensional pattern on the wafer, rather than using a purely linear filter bank. A second option would be to decrease the spacing between resonators from $3\lambda/4$ to $\lambda/4$. In this case, the overall length would only be 1.8 times greater than the current 50 channel prototype and one would expect only a 5% variation in T_c. A 5% variation in T_c across the filter bank will correspond to a 20% variation in responsivity. The detectors must be sufficiently sensitive to achieve background-limited sensitivity for even those detectors with the lowest responsivity.

3. RESONATOR FREQUENCY SCATTER

The readout frequencies of the KIDs exhibit scatter that is not entirely explained by T_c variations. Thus it is important to examine the scatter in resonant frequency in its entirety. The total resonator readout frequency scatter is important because each spectrometer will require hundreds of detectors. If the resonators exhibit too much scatter from their targeted values, there will be collisions between resonators in frequency space resulting in unusable channels lowering the effective yield. Figure 3 (A) shows the measured readout frequency versus the designed readout frequency for the latest filter bank prototype. The measured resonator frequencies came out a factor ∼1.25 times greater than the designed values. This is consistent with the 1.55 times increase in T_c measured for this chip. Three diagnostic channels are shown at the lowest frequencies and the 50 spectral filter bank channels are grouped in four banks in readout frequency space. For each of the four banks the resonators are monotonically increasing in distance along the filter bank.

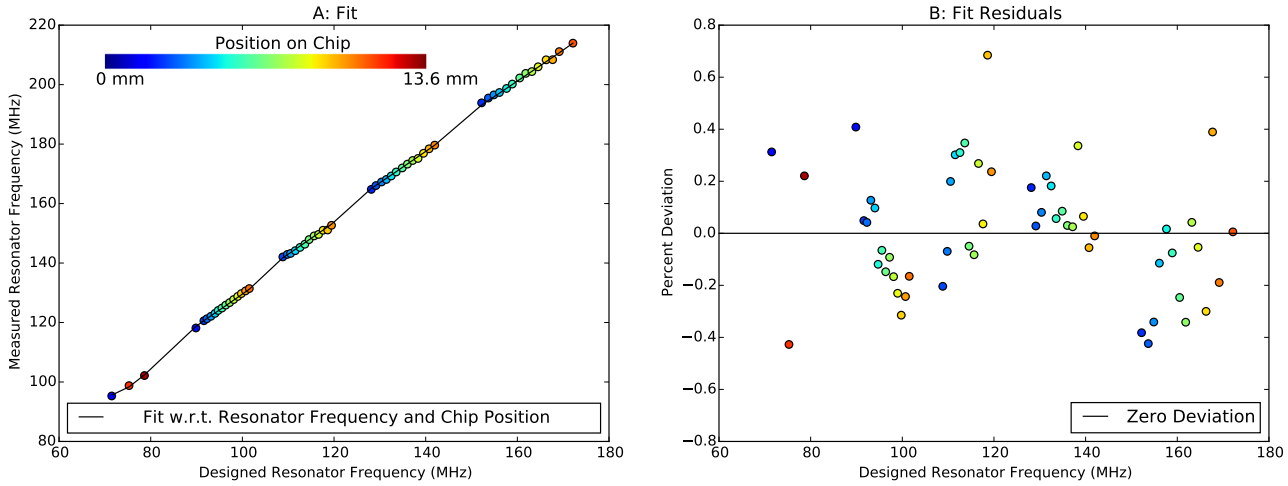

Figure 3. (A) Designed resonator frequency versus measured resonator frequency (colored circles) with a fit (black line). The fit is both a second order polynomial with respect to designed readout frequency and linear fit with respect to the location of the resonator on the chip (B) Residuals of the fit after fitted function is removed.

In order to remove systematic trends with readout frequency and position on the chip so that the random scatter can be measured, a 2^{nd} order polynomial function with readout frequency and a linear function with distance along the filter bank is fit simultaneously. The function is then subtracted to obtain the residuals plotted in Figure 3 (B), which indicate a $\sigma = 0.23\%$ random scatter. The current devices have $Q_r = 10^{4.2}$, while $Q_r = 10^5$ will be targeted for the full filter bank. With the value of $Q_r = 10^5$ the resonant frequency scatter corresponds to an expected collision rate of 1.5%, for a full N=280 detector device when using one octave of readout bandwidth, where a collision is defined as two resonators being within 5 FWHM of each other. This is shown in blue in Figure 4. In the current filterbank design adjacent spectral channels overlap, so any given

optical frequency is sampled by multiple channels. A loss of up to 1.5% of the channels will therefore have a negligible effect on the spectral coverage of the full filter bank.

Systematic scalings to the resonator readout frequencies with respect to chip position and readout frequency will also effect the number of collisions. We minimize this effect by placing nearest neighbors in readout space nearly adjacent in physical space; for this filter bank the spacing was 1 mm on the chip. The systematic scaling of resonator frequency with chip position corresponded to a 150 kHz shift over this same length scale. For a future full filter bank, N = 280 detectors, using 1 octave of bandwidth the spacing would be on the order of 360 kHz. For $Q_r = 10^5$ the FWHM of each resonator is 2 kHz. A 150 kHz shift between adjacent resonators will therefore still leave these resonators well-separated, and is not expected to generate any collisions.

For the scaling with readout frequency the fit was dominated by the linear term. Considering the slope of this linear fit, we can approximate the effect of this systematic trend on collisions. A slope greater than unity will drive the resonator frequencies further apart, decreasing collisions and increasing the required bandwidth. A slope that is less than unity will increase the number of collisions and decrease the required bandwidth. For this device the slope was 1.2, increasing the required bandwidth by that factor and decreasing the number of collisions by $1/1.2 = \sim 0.8$. For the previous dark device we had a slope of 0.9 which decreased the required bandwidth by that factor and increased the collision probability by a factor of ~ 1.1. SuperSpec's resonators are read out in the 50-250 MHz (2.25 octaves of bandwidth) range with a 500 MSamples/s readout. This means that two full devices could be read out in two octaves of bandwidth with a single readout board leaving some extra bandwidth in the case of a systematic scaling that increases the required bandwidth. The effect of a $\pm 25\%$ systematic change in the effective bandwidth on the collision probability is shown in grey in Figure 4.

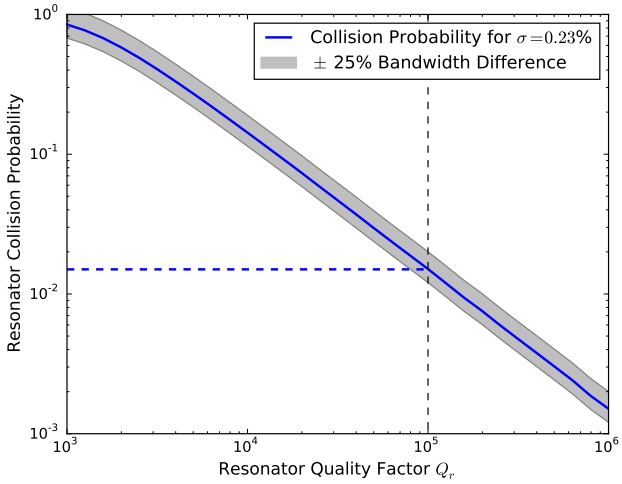

Figure 4. Collision probability for a random scatter in resonant frequencies of $\sigma = 0.23\%$ using one octave of readout bandwidth. The effect of increasing or decreasing the readout bandwidth by a factor 25% is shown in grey.

4. MM-WAVE RESONATOR FREQUENCY SCATTER

For the mm-wave resonant filters minimal scatter in frequency is desired so that channels do not overlap or spread apart, opening gaps in the spectral coverage. The mm-wave profiles were determined by scanning a coherent source across the bandwidth of the filter bank while simultaneously reading out all of the resonators using a CASPER-ROACH based FPGA multitone readout. A large dynamic range is required to simultaneously read out the spectral channels (large response) and broadband channels (small response) at the front and end of the line. In order to accomplish this a comb of tones spanning 90 kHz (10s of FWHMs) to readout each resonator was used. That way when a resonator shifts away from one tone by more than its linewidth it can be read out with the adjacent tone. As a result data for two sets of resonators that were within 90 kHz of each other was not obtained and thus four filterbank channels are not shown in Figure 1 and Figure 5. To remove the

transfer function of the system optics, the response of each spectral channel was normalized by the response of a broadband absorber located on the microstrip line before any of the resonant filters (Figure 1). A Lorentzian was then fit to each channel's profile to determine the measured mm-wave spectral frequency of each channel.

A linear function is fit to these data as shown in Figure 5 (A). The center of the filter bank was shifted by 2 GHz. This means that there is a small systematic shift of the entire filter bank in mm-wave frequency space. An implication of this is that a full filter bank will require additional channels at high and low frequencies so that if there is a systematic shift to higher or lower filter frequencies there will still be complete coverage across the scientific band of interest. The slope of the fit, 1.05, causes a systematic spreading of the filter channels. However this 1.05 systematic spreading is a subdominant effect to the random scatter, shown in Figure 5 (B). The residual scatter is 0.04% compared to the filter spacing that is 0.17%. This suggests that for an N=280 device the mm-wave frequency scatter will have a negligible affect on the spectral coverage.

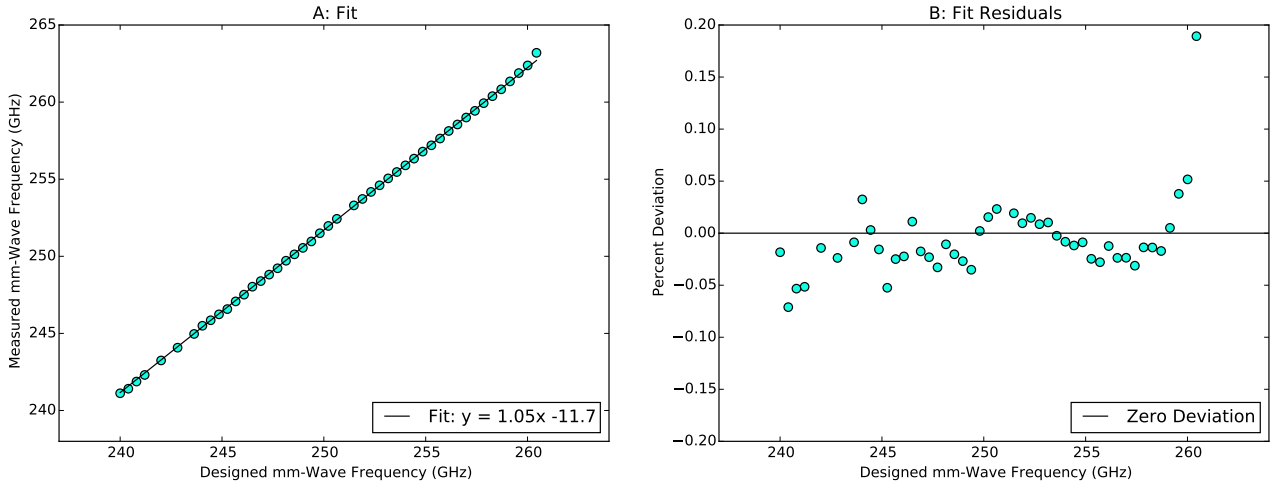

Figure 5. (A) Designed mm-wave resonant filter frequencies versus measured mm-wave resonant filter frequencies (circles) with a fit (black line). (B) Residuals of the fit.

5. EVIDENCE FOR G-R NOISE

In Figure 6 we show noise PSDs obtained on a dark SuperSpec detector with $T_c = 1.2$ K, over a range of stage temperatures. At high temperatures the noise is white and increases rapidly with temperature, as expected for thermal G-R noise. For G-R noise we expect:

$$S_{xx}^{GR} = 4 \cdot \frac{n_{qp}}{V} \cdot \tau_{qp} \cdot \left(\frac{dx}{dn_{qp}}\right)^2, \text{ where } dx = \frac{df_r}{f_r} \tag{1}$$

with,

$$n_{qp} = 2 \cdot N_0 \cdot \sqrt{2\pi\Delta_0 k_B T} \cdot e^{-\Delta_0/(k_B T)} + \cdot n_{qp-min} \tag{2}$$

where the first term above is the density of quasiparticles due to thermal fluctuations, and the second accounts for an excess quasiparticle population remaining at zero temperature. In Figure 6 (B) we fit the temperature dependence of S_{xx} with this expression, holding τ_{qp} independent of temperature,[8,9] assuming $N_0 = 4 \cdot 10^{10}$ eV$^{-1}\mu$m^{-3}, and using Mattis-Bardeen theory to compute $\frac{df/f}{dn_{qp}}$.[10] A best fit is found for $\tau_{qp} = 8.4$ μs and $n_{qp-min} = 1800$ μm^{-3}. This value of τ_{qp} is roughly consistent with previous findings for TiN.[11] Since the roll-off in the PSD is dominated by the resonator ring-down time, there is not a more direct way to measure τ_{qp}, meaning the accuracy of this method of measuring τ_{qp} is unable to be confirmed. However, as the trend with temperature is well described by a reasonable τ_{qp}, we believe the detectors are G-R noise limited above T $\sim$ 250 mK.

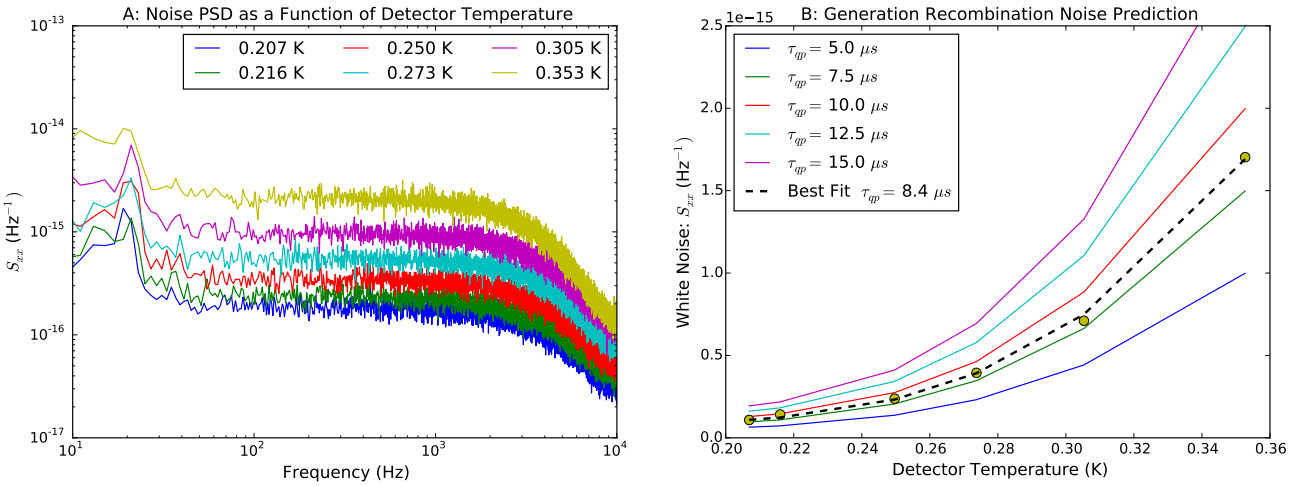

Figure 6. (A) Noise PSD as a function of array temperature. (B) The prediction of G-R noise as a function of array temperature for several constant τ_{qp} values along with the best fit value.

At lower temperatures the noise reaches a floor in excess of the predicted thermal G-R noise. The fit described above suggests this noise floor can be modeled as G-R noise associated with fluctuations in the quasiparticle density that yield a minimum quasiparticle density n_{qp-min}. The noise PSD remains white at low temperatures, and for different detectors on the same device with different volumes we find $S_{xx} \sim V^{-1}$, in both cases supporting the G-R noise interpretation.

6. NOISE EQUIVALENT POWER

For the most recent device the responsivity was found by measuring the change in white S_{xx} photon noise in the detectors as the loading of a coherent source was varied. The responsivity, R, can be extracted from the slope of the measurement using the equation $dS_{xx}/dP = 4R^2h\nu$.[6] This is shown in Figure 7 (A). This responsivity, $R = 1.7 \cdot 10^8$ W^{-1}, along with the measured S_{xx} value for the most recent $T_c = 1.85$ K chip, produces a NEP curve represented by the blue curve in Figure 7 (B). This responsivity is not what one would expect for a future SuperSpec filter bank with $T_c = 1.2$ K. Thus in order to estimate the NEP for a $T_c = 1.2$ K chip, the previously measured responsivity for a $T_c = 1.15$ K device, $R = 9.8 \cdot 10^8$ W^{-1},[6] is used, along with dark noise data taken on the previous optically dark $T_c = 1.2$ K chip, for which the median white noise level at 100-200 Hz was $S_{xx} = 5 \cdot 10^{-17}$ Hz^{-1}. This produces a NEP that is $7 \cdot 10^{-18}$ WHz$^{-0.5}$ which is represented by the curve shown in green in Figure 7 (B). The fact that the responsivity for the $T_c = 1.85$ K chip was a factor of 5.8 times less than the responsivity of the previous $T_c = 1.15$ K chip is roughly consistent with the 5.3 times decrease expected when comparing T_c values.

The current NEP level is sufficient to do ground-based spectroscopy at R = 100 (red dashed line Figure in 7 (B)); however, further reduction is required to meet the background limit for R = 400 spectroscopy (purple dashed line in Figure 7 (B)). In order to meet the R = 400 requirement we could further reduce the inductor volume of the detectors.

7. CONCLUSIONS

SuperSpec is an on-chip spectrometer technology that will enable the production of small profile submm/mm-wave survey spectrometers. The goal of the SuperSpec project is to produce a background-limited prototype for either R = 100, or R = 400 ground-based spectroscopy covering the 190-310 GHz atmospheric window. A 50 channel subset of a full 280 channel filter bank has recently been fabricated and tested. The test device had a 100% yield. The testing of this device is informing of potential design modifications to produce a full scale background-limited filter bank chip with high effective yield.

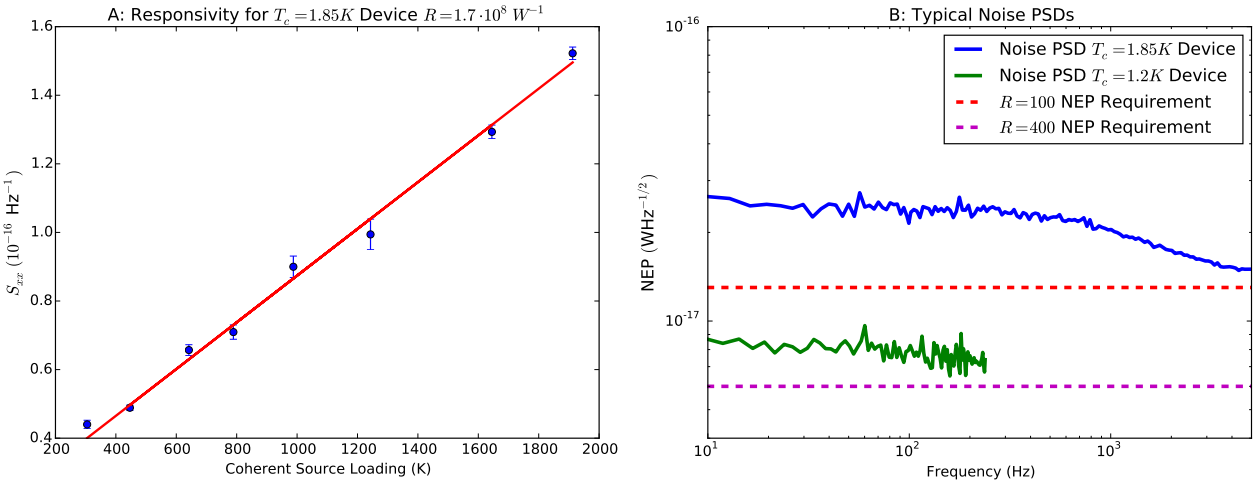

Figure 7. (A) Photon noise from a coherent local oscillator source as a function of loading for the most recent $T_c = 1.85$ K chip, yielding a responsivity of $R = 1.7 \cdot 10^8$ W^{-1} (B) Typical noise PSDs for SuperSpec detectors. Blue indicates the NEP for a $T_c = 1.85$ K chip and green indicates NEP for a $T_c = 1.2$ K chip.

T_c variation across the chip can increase the collision rate and will cause responsivity variations across the filter bank. By switching to a $\lambda/4$ from a $3\lambda/4$ filter spacing the T_c variation can be decreased, minimizing collisions and capping the responsivity variation to 20%. Analysis of the scatter in resonator readout frequency values indicates that there will only be a few collisions when scaled up to a full filter bank. The mm-wave resonant filter frequency scatter is significantly less than the line widths of the resonant filters indicating that for an N=280 device the mm-wave frequency scatter will have a negligible affect on the spectral coverage.

It is believed that the noise performance is currently limited by generation-recombination noise. With the current detector design, NEPs of $7 \cdot 10^{-18}$ WHz$^{-0.5}$ are expected for $T_c = 1.2$ K devices, achieving near background-limited performance at R = 400 and already meeting the R = 100 requirement. Further improvement to NEP can be made by decreasing the inductor volume. In conclusion, a full scale R = 100 or R = 400 background-limited filter bank with high effective yield can be produced and some potential design modifications have been established that will help achieve that goal.

ACKNOWLEDGMENTS

This work is supported in part by NASA Space Technology Research Fellowship NSTRF NNX15AQ09H and NSF AST ATI grant 1407457.

REFERENCES

[1] Glenn, J., Conley, A., Bthermin, M., Altieri, B., Amblard, A., Arumugam, V., Aussel, H., Babbedge, T., Blain, A., Bock, J., Boselli, A., Buat, V., Castro-Rodrguez, N., Cava, A., Chanial, P., Clements, D. L., Conversi, L., Cooray, A., Dowell, C. D., Dwek, E., Eales, S., Elbaz, D., Ellsworth-Bowers, T. P., Fox, M., Franceschini, A., Gear, W., Griffin, M., Halpern, M., Hatziminaoglou, E., Ibar, E., Isaak, K., Ivison, R. J., Lagache, G., Laurent, G., Levenson, L., Lu, N., Madden, S., Maffei, B., Mainetti, G., Marchetti, L., Marsden, G., Nguyen, H. T., O'Halloran, B., Oliver, S. J., Omont, A., Page, M. J., Panuzzo, P., Papageorgiou, A., Pearson, C. P., Prez-Fournon, I., Pohlen, M., Rigopoulou, D., Rizzo, D., Roseboom, I. G., Rowan-Robinson, M., Portal, M. S., Schulz, B., Scott, D., Seymour, N., Shupe, D. L., Smith, A. J., Stevens, J. A., Symeonidis, M., Trichas, M., Tugwell, K. E., Vaccari, M., Valtchanov, I., Vieira, J. D., Vigroux, L., Wang, L., Ward, R., Wright, G., Xu, C. K., and Zemcov, M., "Hermes: deep galaxy number counts from a p(d) fluctuation analysis of spire science demonstration phase observations," *Monthly Notices of the Royal Astronomical Society* **409**(1), 109–121 (2010).

[2] Kamenetzky, J., Glenn, J., Rangwala, N., Maloney, P., Bradford, M., Wilson, C. D., Bendo, G. J., Baes, M., Boselli, A., Cooray, A., Isaak, K. G., Lebouteiller, V., Madden, S., Panuzzo, P., Schirm, M. R. P., Spinoglio, L., and Wu, R., "Herschel-spire imaging spectroscopy of molecular gas in m82," *The Astrophysical Journal* **753**(1), 70 (2012).

[3] Salvaterra, R., Ferrara, A., and Dayal, P., "Simulating high-redshift galaxies," *Monthly Notices of the Royal Astronomical Society* **414**(2), 847–859 (2011).

[4] Crites, A. T., Bock, J. J., Bradford, C. M., Chang, T. C., Cooray, A. R., Duband, L., Gong, Y., Hailey-Dunsheath, S., Hunacek, J., Koch, P. M., Li, C. T., O'Brient, R. C., Prouve, T., Shirokoff, E., Silva, M. B., Staniszewski, Z., Uzgil, B., and Zemcov, M., "The time-pilot intensity mapping experiment," *Proc. SPIE* **9153**, 91531W–91531W–9 (2014).

[5] Kovcs, A., Barry, P. S., Bradford, C. M., Chattopadhyay, G., Day, P., Doyle, S., Hailey-Dunsheath, S., Hollister, M., McKenney, C., LeDuc, H. G., Llombart, N., Marrone, D. P., Mauskopf, P., O'Brient, R. C., Padin, S., Swenson, L. J., and Zmuidzinas, J., "Superspec: design concept and circuit simulations," *Proc. SPIE* **8452**, 84522G–84522G–10 (2012).

[6] Hailey-Dunsheath, S., Shirokoff, E., Barry, P. S., Bradford, C. M., Chapman, S., Che, G., Glenn, J., Hollister, M., Kovács, A., LeDuc, H. G., Mauskopf, P., McKenney, C., O'Brient, R., Padin, S., Reck, T., Shiu, C., Tucker, C. E., Wheeler, J., Williamson, R., and Zmuidzinas, J., "Low noise titanium nitride kids for superspec: A millimeter-wave on-chip spectrometer," *Journal of Low Temperature Physics* **184**(1), 180–187 (2016).

[7] Vissers, M. R., Gao, J., Sandberg, M., Duff, S. M., Wisbey, D. S., Irwin, K. D., and Pappas, D. P., "Proximity-coupled ti/tin multilayers for use in kinetic inductance detectors," *Applied Physics Letters* **102**(23) (2013).

[8] Hailey-Dunsheath, S., Shirokoff, E., Barry, P. S., Bradford, C. M., Chattopadhyay, G., Day, P., Doyle, S., Hollister, M., Kovacs, A., LeDuc, H. G., Mauskopf, P., McKenney, C. M., Monroe, R., O'Brient, R., Padin, S., Reck, T., Swenson, L., Tucker, C. E., and Zmuidzinas, J., "Status of superspec: a broadband, on-chip millimeter-wave spectrometer," (2014).

[9] Hubmayr, J., Beall, J., Becker, D., Cho, H.-M., Devlin, M., Dober, B., Groppi, C., Hilton, G. C., Irwin, K. D., Li, D., Mauskopf, P., Pappas, D. P., Van Lanen, J., Vissers, M. R., Wang, Y., Wei, L. F., and Gao, J., "Photon-noise limited sensitivity in titanium nitride kinetic inductance detectors," *Applied Physics Letters* **106**(7) (2015).

[10] Gao, J., Zmuidzinas, J., Vayonakis, A., Day, P., Mazin, B., and Leduc, H., "Equivalence of the effects on the complex conductivity of superconductor due to temperature change and external pair breaking," *Journal of Low Temperature Physics* **151**(1-2), 557–563 (2008).

[11] Gao, J., Vissers, M. R., Sandberg, M. O., da Silva, F. C. S., Nam, S. W., Pappas, D. P., Wisbey, D. S., Langman, E. C., Meeker, S. R., Mazin, B. A., Leduc, H. G., Zmuidzinas, J., and Irwin, K. D., "A titanium-nitride near-infrared kinetic inductance photon-counting detector and its anomalous electrodynamics," *Applied Physics Letters* **101**(14) (2012).